Inorg. Chem. **2006**, *45*, 7612−7620

Tuning the Structural and Magnetic Properties of Thermally Robust Coordination Polymers

Norberto Masciocchi,[†] Simona Galli,*[,†] Angelo Sironi,[‡] Elena Cariati,[§] Miguel A. Galindo,[||] Elisa Barea,[§] Mª Angustias Romero,[||] Juan M. Salas,[||] Jorge A. R. Navarro,*[,||] and Francisco Santoyo-González[||]

Dipartimento di Scienze Chimiche e Ambientali, Università dell'Insubria, Via Valleggio 11, 22100 Como, Italy, Dipartimento di Chimica Strutturale e Stereochimica Inorganica, Università di Milano and Istituto di Scienze e Tecnologie Molecolari del CNR (ISTM-CNR), Via Venezian 21, 20133 Milano, Italy, Dipartimento di Chimica Inorganica, Metallorganica e Analitica, Università di Milano and Istituto di Scienze e Tecnologie Molecolari del CNR (ISTM-CNR), Via Venezian 21, 20133 Milano, Italy, and Departamentos de Química Inorgánica y Orgánica, Universidad de Granada, Av. Fuentenueva S/N, 18071 Granada, Spain

Received February 8, 2006

Thermally robust materials of the M(5-X-pyrimidin-2-olate)$_2$ type [M = Co, X = Cl (**1**$_{Cl}$), X = Br (**1**$_{Br}$), X = I (**1**$_I$); M = Zn, X = Cl (**2**$_{Cl}$), X = Br (**2**$_{Br}$), X = I (**2**$_I$)] have been synthesized. Their X-ray powder diffraction structural characterization has revealed that they crystallize as $I\bar{4}2d$ diamondoid frameworks, isomorphous to those of the pristine [M(pyrimidin-2-olate)$_2$]$_n$ analogues (**1**$_H$, M = Co; **2**$_H$, M = Zn). The magnetic measurements of the **1**$_X$ series at magnetic fields of 100, 300, and 5000 Oe reveal a weak ferromagnetic ordering taking place below the Néel temperature ($T_N \sim 20$ K), arising from spin canting phenomena of the antiferromagnetically coupled cobalt centers. Moreover, magnetic hysteresis studies carried out on the **1**$_X$ series at 2 K reveal a strong dependence of both the coercive field H_{coer} (2500, 1000, 775, and 500 Oe for **1**$_{Br}$, **1**$_{Cl}$, **1**$_I$, and **1**$_H$, respectively) and the remnant magnetization M_{rem} (0.0501 μ_B for **1**$_{Br}$ and **1**$_{Cl}$, 0.0457 μ_B for **1**$_I$, and 0.0358 μ_B for **1**$_H$) on the 5-substituent of the pyrimidin-2-olates. The molecular alloys [Co(5-Y-pyrimidin-2-olate)$_2$] (Y = Cl/Br, **1**$_{Cl/Br}$) and [Co(5-Y′-pyrimidin-2-olate)$_2$] (Y′ = Br/I, **1**$_{Br/I}$) have also been prepared and characterized, proving that they have intermediate properties. These materials combine interesting functional properties, such as chemical inertness, magnetism, photoluminescence, and (although weak) SHG activity.

Introduction

Functional coordination polymers have attracted considerable attention in the past few years because of their wide number of interesting properties.[1] The presence, in these frameworks, of transition metal ions is responsible for the incorporation of magnetic, optical, catalytic, and structural properties.[2,3] Of special interest is the construction of materials possessing simultaneously two or more of the above quoted features.[4]

Diazaaromatic ligands in their deprotonated forms, such as pyrazolates, imidazolates, and pyrimidinolates, have been recently coupled to metal ions in the attempt of preparing homoleptic functional materials lacking counterions in the

* To whom correspondence should be addressed. E-mail: simona.galli@uninsubria.it (S.G.), jarn@ugr.es (J.A.R.N.). Fax: +39-031-326230 (S.G.), +34-958-248526 (J.A.R.N.).

[†] Dipartimento di Scienze Chimiche e Ambientali, Università dell'Insubria.

[‡] Dipartimento di Chimica Strutturale e Stereochimica Inorganica, Università di Milano and Istituto di Scienze e Tecnologie Molecolari del CNR.

[§] Dipartimento di Chimica Inorganica, Metallorganica e Analitica, Università di Milano and Istituto di Scienze e Tecnologie Molecolari del CNR.

[||] Departamentos de Química Inorgánica y Orgánica, Universidad de Granada.

(1) See e.g.: (a) Rowsell, J. L. C.; Yaghi, O. M. *Angew. Chem., Int. Ed.* **2005**, *44*, 4670−4679. (b) Moulton, B.; Zaworotko, M. J. *Curr. Opin. Solid State Mater.* **2002**, *6*, 117−123. (c) Janiak, C. *Angew. Chem., Int. Ed. Engl.* **1997**, *36*, 1431−1434.

(2) (a) Janiak, C. *Dalton Trans.* **2003**, 2781−2804. (b) Evans, O. R.; Lin, W. *Acc. Chem. Res.* **2002**, *35*, 511−522. (c) Hagrman, P. J.; Hagrman, D.; Zubieta, J. *Angew. Chem., Int. Ed.* **1999**, *38*, 2638−2684.

(3) Kitagawa, S.; Kitaura, R.; Noro, S.-I. *Angew. Chem., Int. Ed.* **2004**, *43*, 2334−2375.

(4) See e.g.: (a) Benard, S.; Yu, P.; Audiere, J. P.; Riviere, E.; Clement, R.; Guilhem, J.; Tchertanov, L.; Nakatani, K. *J. Am. Chem. Soc.* **2000**, *122*, 9444−9454. (b) Bénard, S.; Rivière, E.; Yu, P.; Nakatani, K.; Delouis, J.-F. *Chem. Mater.* **2001**, *13*, 159−162. (c) Lacroix, P. G.; Malfant, I.; Bénard, S.; Yu, P.; Rivière, E.; Nakatani, K. *Chem. Mater.* **2001**, *13*, 441−449.

10.1021/ic0602188 CCC: $33.50
Published on Web 08/15/2006

Chart 1

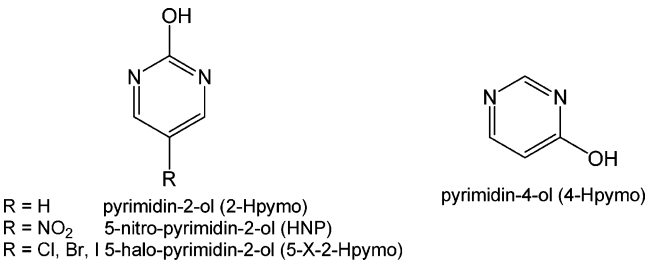

R = H pyrimidin-2-ol (2-Hpymo)
R = NO_2 5-nitro-pyrimidin-2-ol (HNP)
R = Cl, Br, I 5-halo-pyrimidin-2-ol (5-X-2-Hpymo)

pyrimidin-4-ol (4-Hpymo)

crystal lattice, thus inducing mechanical rigidity and, possibly, microporous features.[5,6] As recent examples of the versatility and functional activity of polymeric species of this class, the vapochromic Cu(II) pyrazolates,[7] the microporous Cu(II)[8,9] and Pd(II)[10] pyrimidinolates (capable of selective solid−gas and solid−liquid adsorption processes), the antimicrobic silver imidazolate,[11] and the low κ "dielectric" zinc imidazolate,[12] are here mentioned.

After having extensively studied the realm of metal pyrazolates and imidazolates, we turned our attention to pyrimidin-*n*-ols ($n = 2$ or 4; see Chart 1) and discovered a number of interesting structural and functional features of metal pyrimidinolates, ranging from sorption behavior,[8,9,10] molecular magnetism,[13] and ordered cocrystallization of cyclic oligomers and infinite helices[14] to reversible ring-opening polymerization of cyclohexanuclear moieties assisted by moisture.[15]

Among the samples studied by us in the recent past, thermally robust three-dimensional polymers were prepared, namely the $[M(2\text{-pymo})_2]_n$ species (M = Co, Ni, and Zn), with decomposition temperatures as high as 570 °C in the case of M = Zn.[16] In addition to its unusual high thermal stability, the cobalt derivative was found to exhibit weak SHG properties[16] and to act as a molecular magnet at low temperatures, due to spin-canting of antiferromagnetically coupled Co(II) ions.[13]

In this paper, we report the preparation, the X-ray powder diffraction (XRPD) structural characterization (Table 1), and the thermal, optical, and magnetic properties of the analogous three-dimensional species, assembled by employing the 5-substituted halopyrimidinolates (Chart 1), aiming to finely tune the behavior of this kind of materials by introducing a series of electron-withdrawing atoms in the *para*-position to the exocyclic oxygen atom of the ligand; a similar approach was indeed employed by Le Bideau et al. in vanadyl-based layered species.[17] Indeed, the weak ferromagnetic ordering taking place at low temperature shows an interesting dependence on the halide nature.

Experimental Section

Materials and Physical Measurements. 2-Hydroxypyrimidine·HCl, *N*-bromosuccinimide, and *N*-iodosuccinimide were purchased from Aldrich. $[Co(2\text{-pymo})_2]_n$ (**1_H**),[16] $[Zn(2\text{-pymo})_2]_n$ (**2_H**),[16] 5-chloro-2-hydroxypyrimidine,[18] 5-bromo-2-hydroxypyrimidine, and 5-iodo-2-hydroxypyrimidine[19] were prepared according to literature methods.

Microanalyses of C, H, and N were performed with a Fisons-Instruments EA-1008 analyzer. Thermogravimetric and differential scanning calorimetric analyses were performed, under a reactive atmosphere of air, on Shimadzu-TGA-50H/DSC equipment, at heating rates of 20 and 10 °C min^{-1}, respectively (Scientific Instrumentation Centre of the University of Granada). Electronic spectra on polycrystalline samples were carried out on a Varian Cary UV−vis−NIR spectrophotometer in the reflectance mode (Scientific Instrumentation Centre of the University of Granada). IR spectra were recorded on a Midac FT-IR using KBr pellets. Magnetic susceptibility measurements were performed on polycrystalline samples in the 2−250 K with a quantum design MPMS XL squid in the field-cooled mode by applying 100, 300, and 5000 Oe. Hysteresis loops were measured at 2 K in the −50 to 50 kOe range. Ac magnetic susceptibility measurements were performed in the 2−30 K temperature range in a 1 Oe oscillating field at 1200 Hz. Room-temperature, solid-state emission spectra were recorded using a Jobin Yvon Fluorolog 3 spectrofluorometer equipped with a Hamamatsu R 928 P photomultiplier tube, exciting at 350 nm.

Second-Order NLO Kurtz−Perry Measurements. The 1064 nm initial wavelength of a Nd:YAG pulsed laser beam was shifted to 1907 nm by stimulated scattering in a high-pressure hydrogen cell. A portion of this beam was directed on sample-containing capillaries. The scattered radiation was collected by an elliptical mirror, filtered to select only the second-order contribution, and recollected with a Hamamatsu R5108 photomultiplier tube. The SHG efficiency was evaluated by taking as reference the SHG signal of urea.

Preparation of $[(Co(5\text{-X-2-pymo})_2]_n$. $[(Co(5\text{-Cl-2-pymo})_2]_n$ (**1_{Cl}**), $[(Co(5\text{-Br-2-pymo})_2]_n$ (**1_{Br}**), and $[(Co(5\text{-I-2-pymo})_2]_n$ (**1_I**) have been prepared by following a similar synthetic route: 2 mmol of $CoCl_2 \cdot 6H_2O$ was dissolved in distilled water (10 mL), and the corresponding 5-halo-2-hydroxypyrimidine (4 mmol dissolved in 50 mL of water) was added under stirring. The clear solutions were kept at room temperature for about 20 min, and then the pH was raised to 5.0 by addition of 1 M NaOH. The purple $[Co(5\text{-X-2-pymo})_2]_n$ precipitates (**1_{Cl}**, **1_{Br}**, **1_I**) were filtered off and washed

(5) Tian, Y.-Q.; Cai, C.-X.; Ren, X.-M.; Duan, C.-Y.; Xu, Y.; Gao, S.; You, X.-Z. *Chem.*—Eur. J. **2003**, *9*, 5673−5685.
(6) Navarro, J. A. R.; Barea, E.; Galindo, M. A.; Salas, J. M.; Romero, M. A.; Quirós, M.; Masciocchi, N.; Galli, S.; Sironi, A.; Lippert, B. *J. Solid State Chem.* **2005**, *178*, 2436−2451.
(7) Cingolani, A.; Galli, S.; Masciocchi, N.; Pandolfo, L.; Pettinari, C.; Sironi, A. *J. Am. Chem. Soc.* **2005**, *127*, 6144−6145.
(8) (a) Tabares, L. C.; Navarro, J. A. R.; Salas, J. M. *J. Am. Chem. Soc.* **2001**, *123*, 383−387. (b) Barea, E.; Navarro, J. A. R.; Salas, J. M.; Masciocchi, N.; Galli, S.; Sironi, A. *Polyhedron* **2003**, 22, 3051−3057. (c) Barea, E.; Navarro, J. A. R.; Salas, J. M.; Quirós, M. *Dalton Trans.* **2005**, 1743−1746.
(9) Barea, E.; Navarro, J. A. R.; Salas, J. M.; Masciocchi, N.; Galli, S.; Sironi, A. *J. Am. Chem. Soc.* **2004**, *126*, 3014−3015.
(10) Navarro, J. A. R.; Barea, E.; Salas, J. M.; Masciocchi, N.; Galli, S.; Sironi, A.; Ania, C. O.; Parra, J. B. *Inorg. Chem.* **2006**, *45*, 2397−2399.
(11) Nomiya, K.; Tsuda, K.; Sudoh, T.; Oda, M. *J. Inorg. Biochem.* **1997**, *68*, 39−44.
(12) Świątek-Tran, B.; Kołodziej, H. A.; Tran, V. H. *J. Solid State Chem.* **2004**, 177, 1011−1016.
(13) Masciocchi, N.; Galli, S.; Sironi, A.; Barea, E.; Navarro, J. A. R.; Salas, J. M.; Tabares, L. C. *Chem. Mater.* **2003**, *15*, 2153-2160.
(14) Masciocchi, N.; Ardizzoia, G. A.; La Monica, G.; Maspero, A.; Sironi, A. *Angew. Chem., Int. Ed.* **1998**, *37*, 3366−3369.
(15) Masciocchi, N.; Moret, M.; Corradi, E.; Ardizzoia, G. A.; Maspero, A.; La Monica, G.; Sironi, A. *Inorg. Chem.* **1997**, *36*, 5648−5650.
(16) Masciocchi, N.; Ardizzoia, G. A.; LaMonica, G.; Maspero, A.; Sironi, A. *Eur. J. Inorg. Chem.* **2000**, 2507−2515.
(17) Le Bideau, J.; Papoutsakis, D.; Jackson, J. E.; Nocera, D. G. *J. Am. Chem. Soc.* **1997**, *119*, 1313−1316.
(18) Crosby, D. G.; Berthold, R. V. *J. Org. Chem.* **1960**, *25*, 1916−1919.
(19) Efange, S. M. N.; Alessi, E. M.; Shih, H. C.; Cheng, Y. C.; Bardos, T. J. *J. Med. Chem.* **1985**, *28*, 904−910.

Table 1. Crystal Data and Refinement Details for Compounds $[Co(5\text{-Cl-2-pymo})_2]_n$ (**1$_{Cl}$**), $[Co(5\text{-Br-2-pymo})_2]_n$ (**1$_{Br}$**), $[Co(5\text{-I-2-pymo})_2]_n$ (**1$_I$**), $[Zn(5\text{-Cl-2-pymo})_2]_n$ (**2$_{Cl}$**), $[Zn(5\text{-Br-2-pymo})_2]_n$ (**2$_{Br}$**), and $[Zn(5\text{-I-2-pymo})_2]_n$ (**2$_I$**)

param	**1$_{Cl}$**	**1$_{Br}$**	**1$_I$**	**2$_{Cl}$**	**2$_{Br}$**	**2$_I$**
indexing method	SVD[20]	SVD[20]	SVD[20]	SVD[20]	SVD[20]	SVD[20]
indexing FoM	$M(14)^{22} = 19$	$M(16)^{22} = 55$	$M(20)^{22} = 24$	$M(13)^{22} = 69$	$M(13)^{22} = 43$	$M(13)^{22} = 48$
system	tetragonal	tetragonal	tetragonal	tetragonal	tetragonal	tetragonal
SPGR, Z	$I\bar{4}2d$, 4	$I\bar{4}2d$, 4	$I\bar{4}2d$, 4	$I\bar{4}2d$, 4	$I\bar{4}2d$, 4	$I\bar{4}2d$, 4
a, Å	8.5489(1)	8.6844(2)	8.9775(3)	8.5561(2)	8.6900(3)	8.9603(4)
c, Å	15.1178(3)	14.9105(4)	14.8646(6)	15.3269(5)	15.1505(6)	14.9706(9)
V, Å^3	1104.88(5)	1124.54(5)	1198.02(2)	1122.04(6)	1144.26(9)	1202.2(1)
fw	317.98	406.89	500.89	324.44	413.34	507.34
ρ_{calc}, g cm^{-3}	1.912	2.403	2.778	1.921	2.400	2.805
$F(000)$	628	772	916	640	784	928
μ(Cu Kα), cm^{-1}	166.5	203.4	518.8	74.4	112.0	433.5
diffractometer	Bruker D8	Bruker D8	Bruker D8	Bruker D8	Bruker D8	Bruker D8
T, K	298(2)	298(2)	298(2)	298(2)	298(2)	298(2)
measd 2θ range, deg	5−105	5−105	5−105	5−105	5−105	5−105
N_{data}	5001	5001	5001	5001	5001	5001
N_{obs}	191	195	208	196	200	211
R_p, R_{wps}	0.094, 0.116	0.094, 0.122	0.113, 0.150	0.091, 0.116	0.075, 0.098	0.082, 0.109
R_{Bragg}[a]	6.441	6.014	5.651	6.231	4.970	2.868
χ^2 [a]	1.443	1.548	1.340	1.716	1.737	1.292
V/Z, Å^3	276.2	281.1	299.5	280.5	286.1	300.5

[a] $R_p = \sum_i|y_{i,o} - y_{i,c}|/\sum_i|y_{i,o}|$; $R_{wp} = [\sum_i w_i(y_{i,o} - y_{i,c})^2/\sum_i w_i(y_{i,o})^2]^{1/2}$; $R_{Bragg} = \sum_n|I_{n,o} - I_{n,c}|/\sum_n I_{n,o}$; $\chi^2 = \sum_i w_i(y_{i,o} - y_{i,c})^2/(N_{obs} - N_{par})$, where $y_{i,o}$ and $y_{i,c}$ are the observed and calculated profile intensities, respectively, while $I_{n,o}$ and $I_{n,c}$ the observed and calculated intensities. The summations run over i data points or n independent reflections. Statistical weights w_i are normally taken as $1/y_{i,o}$.

with water, ethanol, and ether. In the synthesis of the molecular alloys **1$_{Cl/Br}$** and **1$_{Br/I}$**, an aqueous solution containing 1 mmol of $CoCl_2 \cdot 6H_2O$ was mixed with another one containing 2 mmol of a 1:1 mixture of the corresponding 5-halo-2-pymo derivatives; after posterior addition of NaOH the corresponding products were filtered off.

1$_{Cl}$. Yield: 90%. Anal. Calcd for $C_8H_4Cl_2CoN_4O_2$: C, 30.21; H, 1.26; N, 17.61. Found: C, 30.03; H, 1.13; N, 17.59. IR (ν, cm^{-1}): 1628 vs, 1601 s, 1582 s, 1527 vs, 1363 s, 1252 s, 1163 m, 804 m, 731 m, 703 m. UV−vis (cm^{-1}): 30 490 (s), 18 250 (s, $^4A_2 \rightarrow {}^4T_1$(P)), 9390 (s, $^4A_2 \rightarrow {}^4T_1$).

1$_{Cl/Br}$. Yield: 60%. Anal. Calcd for $C_8H_4BrClCoN_4O_2$: C, 26.51; H, 1.11; N, 15.46. Found: C, 26.57; H, 1.02; N, 15.36. IR (ν, cm^{-1}): 1625 vs, 1600 s, 1579 s, 1524 vs, 1363 s, 1263 s, 1253 vs, 1162 m, 1145 m, 803 m, 731 m, 701 m. UV−vis (cm^{-1}): 30 210 (s), 18 250 (s, $^4A_2 \rightarrow {}^4T_1$(P)), 9415 (s, $^4A_2 \rightarrow {}^4T_1$).

1$_{Br}$. Yield: 85%. Anal. Calcd for $C_8H_4Br_2CoN_4O_2$: C, 23.62; H, 0.99; N, 13.77. Found: C, 23.49; H, 1.12; N, 13.76. IR (ν, cm^{-1}): 1623 vs, 1600 s, 1577 s, 1546 m, 1523 vs, 1363 vs, 1261 vs, 1145 m, 803 m, 699 m. UV−vis (cm^{-1}): 30 030 (s), 18 020 (s, $^4A_2 \rightarrow {}^4T_1$(P)), 9380 (s, $^4A_2 \rightarrow {}^4T_1$).

1$_{Br/I}$. Yield: 60%. Anal. Calcd for $C_8H_4BrCoIN_4O_2$: C, 21.17; H, 0.89; N, 12.34. Found: C, 20.77; H, 0.93; N, 11.89. IR (ν, cm^{-1}): 1618 vs, 1596 s, 1571 s, 1518 vs, 1361 s, 1262 s, 1141 m, 803 m, 698 m. UV−vis (cm^{-1}): 29 940 (s), 18 020 (s, $^4A_2 \rightarrow {}^4T_1$(P)), 9480 (s, $^4A_2 \rightarrow {}^4T_1$).

1$_I$. Yield: 90%. Anal. Calcd for $C_8H_4CoI_2N_4O_2$: C, 19.18; H, 0.80; N, 11.19. Found: C, 19.30; H, 0.83; N, 11.29. IR (ν, cm^{-1}): 1615 vs, 1597 s, 1572 s, 1517 vs, 1366 vs, 1264 vs, 1138 m, 917 m, 803 m, 699 m. UV−vis (cm^{-1}): 28 985 (s), 17 825 (s, $^4A_2 \rightarrow {}^4T_1$(P)), 9200 (s, $^4A_2 \rightarrow {}^4T_1$).

Preparation of $[(Zn(5\text{-X-2-pymo})_2]_n$. $[(Zn(5\text{-Cl-2-pymo})_2]_n$ (**2$_{Cl}$**), $[(Zn(5\text{-Br-2-pymo})_2]_n$ (**2$_{Br}$**), and $[(Zn(5\text{-I-2-pymo})_2]_n$ (**2$_I$**), have been prepared by following the above-mentioned synthetic procedure, starting from $Zn(NO_3)_2 \cdot 6H_2O$.

2$_{Cl}$. Yield: 90%. Anal. Calcd for $C_8H_4Cl_2N_4O_2Zn$: C, 29.62; H, 1.24; N, 17.27. Found: C, 29.43; H, 1.18; N, 17.37. IR (ν, cm^{-1}): 1625 vs, 1601 s, 1584 s, 1525 vs, 1363 s, 1252 s, 1163 m, 803 m, 730 m, 703 m.

2$_{Br}$. Yield: 85%. Anal. Calcd for $C_8H_4Br_2N_4O_2Zn$: C, 23.25; H, 0.98; N, 13.55. Found: C, 23.24; H, 1.05; N, 13.23. IR (ν, cm^{-1}): 1631 vs, 1602 vs, 1583 s, 1524 vs, 1367 vs, 1263 vs, 1146 m, 920 m, 804 m, 698 m.

2$_I$. Yield: 90%. Anal. Calcd for $C_8H_4I_2N_4O_2Zn$: C, 18.93; H, 0.79; N, 11.04. Found: C, 19.09; H, 0.90; N, 11.04. IR (ν, cm^{-1}): 1621 vs, 1599 vs, 1575 s, 1519 vs, 1370 vs, 1266 vs, 1139 m, 920 m, 803 m, 696 m, 650 m.

X-ray Powder Diffraction Analysis of $[Co(5\text{-X-2-pymo})_2]_n$ (1$_X$) and $[Zn(5\text{-X-2-pymo})_2]_n$ (2$_X$). The powders were gently ground in an agate mortar and then deposited with care in the hollow of an aluminum holder equipped with a zero background plate (supplied by The Gem Dugout, State College, PA). Diffraction data (Cu Kα, $\lambda = 1.5418$ Å) were collected on a θ:θ Bruker Axs D8 Advance vertical scan diffractometer, equipped with primary and secondary Soller slits, a secondary beam curved graphite monochromator, a Na(Tl)I scintillation detector, and pulse height amplifier discrimination. The generator was operated at 40 kV and 40 mA. Optics used: divergence slit, 0.5°; antiscatter slit, 0.5°; receiving slit, 0.2 mm. The nominal resolution of the present setup is 0.07° in 2θ for the Si(111) peak at 28.44° (α_1 component). Long scans were performed in the $5 < 2\theta < 105°$ range, with $t = 12$ (**1$_I$**), 14 (**1$_{Br}$** and **2$_{Cl}$**), 16 (**2$_I$**), 17 (**2$_{Br}$**), or 19 (**1$_{Cl}$**) s and $\Delta 2\theta = 0.02°$.

Indexing was obtained with the aid of the single value decomposition approach,[20] as implemented in the TOPAS-R suite of programs[21] [**1$_{Cl}$**, tetragonal, $a = 8.55$ and $c = 15.12$ Å, $V = 1105.6$ Å^3, $M(14)^{22} = 19$; **1$_{Br}$**, tetragonal, $a = 8.69$ and $c = 14.65$ Å, $V = 1129.3$ Å^3, $M(16) = 55$; **1$_I$**, tetragonal, $a = 8.99$ and c 14.87 = Å, $V = 1203.3$ Å^3, $M(20) = 24$; **2$_{Cl}$**, tetragonal, $a = 8.56$ and $c = 15.32$ Å, $V = 1122.1$ Å^3, $M(13) = 69$; **2$_{Br}$**, tetragonal, $a = 8.70$ and $c = 15.16$ Å, $V = 1149.1$ Å^3, $M(13) = 43$; **2$_I$**, tetragonal, $a = 8.96$ and $c = 14.97$ Å, $V = 1201.0$ Å^3, $M(13) = 43$]. Systematic absences indicated $I\bar{4}2d$ as the probable space group for the **1$_X$** and **2$_X$** series (corroborated by the isomorphism with the previously

(20) Coelho, A. A. *J. Appl. Crystallogr.* **2003**, *36*, 86−95.
(21) *Topas-R: General profile and structure analysis software for powder diffraction data*; Bruker AXS, Karlsruhe, Germany, 2001.
(22) De Wolff, P. M. *J. Appl. Crystallogr.* **1968**, *1*, 108−113.

Table 2. Relevant Structural, Thermal, and Spectroscopic Parameters for the Isomorphic (Tetragonal, $I\bar{4}2d$) $[M(5\text{-X-2-pymo})_2]_n$ Species (X = H, Cl, Cl/Br, Br, Br/I, I)

param	$\mathbf{1_H}$	$\mathbf{1_{Cl}}$	$\mathbf{1_{Cl/Br}}$	$\mathbf{1_{Br}}$	$\mathbf{1_{Br/I}}$	$\mathbf{1_I}$	$\mathbf{2_H}$	$\mathbf{2_{Cl}}$	$\mathbf{2_{Br}}$	$\mathbf{2_I}$
a, Å	7.4114(3)	8.5489(1)	8.6281(2)	8.6844(2)	8.8567(2)	8.9775(3)	7.3919(2)	8.5561(2)	8.6900(3)	8.9603(4)
c, Å	17.0879(7)	15.1178(3)	15.0473(4)	14.9105(4)	14.9226(4)	14.8646(6)	17.3389(6)	15.3269(5)	15.1505(6)	14.9706(9)
V, Å^3	938.63(6)	1104.88(5)	1120.18(5)	1124.54(5)	1170.56(7)	1198.02(2)	947.39(5)	1122.04(6)	1144.26(9)	1202.2(1)
V/*Z*	234.7	276.2	280.0	281.1	292.6	299.5	236.85	280.5	286.1	300.5
struct	3D	3D	3D	3D	3D	3D	3D	3D	3D	3D
M stereochem	CoN_4	CoN_4	CoN_4	CoN_4	CoN_4	CoN_4	ZnN_4	ZnN_4	ZnN_4	ZnN_4
M···M, Å	5.655	5.705	5.724	5.722	5.787	5.826	5.696	5.742	5.763	5.837
ligand coord	η^1-*N*,η^1 -*N*′	η^1-*N*,η^1 -*N*′	η^1-*N*,η^1 -*N*′	η^1-*N*,η^1 -*N*′	η^1-*N*,η^1 -*N*′	η^1-*N*,η^1 -*N*′	η^1-*N*,η^1 -*N*′	η^1-*N*,η^1 -*N*′	η^1-*N*,η^1 -*N*′	η^1-*N*,η^1 -*N*′
M−N, Å	2.032(4)	1.985(2)	1.972(2)	1.970(2)	1.998(2)	2.021(1)	2.086(4)	1.990(1)	1.961(1)	2.006(7)
N−M−N, deg	107.2(1)	107.6(9)	108.1(2)	107.2(2)	108.4(2)	108.1(5)	108.0(1)	107(1)	108.6(2)	109.0(2)
	114.0(3)	113.2(2)	112.2(4)	113.2(3)	111.5(4)	110.1(2)	112.5(2)	113.3(2)	111.2(3)	110.4(5)
C−X, Å		1.784	1.784, 1.941	1.941	1.941, 2.113	2.113		1.784	1.941	2.113
O···X, Å		2.789		2.769		2.889		2.797	2.774	2.861
ν(CO), cm^{-1}	1630	1628	1625	1623	1618	1615	1633	1625	1631	1621
Δ_t, cm^{-1}	5500	5540	5560	5550	5620	5544				
μ_{eff}, μ_B	4.45(2)	4.50(2)		4.48(2)		4.54(2)				
T_{dec}, °C	560	420	440	450	385	350	570	410	430	330
Ref	16	this work	this work	this work	this work	this work	16	this work	this work	this work

reported $[M(2\text{-pymo})_2]_n$ species),[16] later confirmed by successful solution and refinement. For the sake of completeness, structure solution and refinement were attempted also in $I4_1md$, which shares the same extinction rules as $I\bar{4}2d$. Yet, even by allowance of a disordered structure to be present, neither a satisfactory model nor low agreement factors were obtained. Structure solutions were performed by using the simulated annealing[23] technique implemented in TOPAS. The 5-X-2-pymo ligands were treated as C_{2v} rigid bodies, with geometrical parameters derived from ab initio quantomechanical computations.[24] The final refinements were performed by the Rietveld method using TOPAS. Peak shapes were described by the fundamental parameters approach.[25] The experimental background was fit by a polynomial description. Systematic errors were modeled with sample-displacement angular shifts, preferred orientation corrections in the March−Dollase[26] formulation (with [011] poles, for $\mathbf{1_{Br}}$, $\mathbf{1_I}$, and $\mathbf{2_I}$), and anisotropic peak shape broadening (for $\mathbf{1_I}$).[25] Metal atoms were given a refinable, isotropic displacement parameter (B_M), while lighter atoms were assigned a common $B = B_M + 2.0$ Å^2 value. Scattering factors, corrected for real and imaginary anomalous dispersion terms, were taken from the internal library of TOPAS.

Final R_p, R_{wp}, R_{Bragg}, and χ^2 agreement factors and details on data collections and analyses for $\mathbf{1_X}$ and $\mathbf{2_X}$ can be found in Tables 1 and 2.

Crystallographic data (excluding structure factors) for the structures reported in this paper have been deposited with the Cambridge Crystallographic Data Centre as supplementary publication Nos. CCDC 293137−293144. Copies of the data can be obtained free of charge on application to CCDC, 12 Union Road, Cambridge CB2 1EZ, U.K. (fax, (+44)1223 336−033; e-mail, deposit@ccdc.cam.ac.uk).

Thermodiffractometric Experiments. The thermal behavior of the $[M(5\text{-X-2-pymo})_2]_n$ species was further studied by employing a custom-made heater (supplied by Officine Elettrotecniche di Tenno, Bleggio Inferiore (TN), Italy), mounted on a Bruker AXS Advance D8 diffractometer. A sequence of consecutive scans in the 17−37° in 2θ range was performed in the 20−440 °C temperature range, with steps of 20 °C. The thermal expansion coefficients have been calculated by taking into account the data acquired up to 340 °C, and the lattice parameters have been derived by whole pattern profile fitting.

Results and Discussion

Synthesis, Spectroscopy, and Thermal Behavior of $[Co(5\text{-X-2-pymo})_2]_n$ ($\mathbf{1_X}$) and $[Zn(5\text{-X-2-pymo})_2]_n$ ($\mathbf{2_X}$). The reaction of the 5-X-2-pymo ligands (5-X-2-pymo = 5-X-pyrimidin-2-olate) with the proper metal salt in an aqueous medium results in the precipitation of microcrystalline powders of $M(5\text{-X-2-pymo})_2$ formula [M = Co, X = Cl ($\mathbf{1_{Cl}}$), X = Br ($\mathbf{1_{Br}}$), X = I ($\mathbf{1_I}$); M = Zn, X = Cl ($\mathbf{2_{Cl}}$), X = Br ($\mathbf{2_{Br}}$), X = I ($\mathbf{2_I}$)]. Analogously, anhydrous species of formula $M(2\text{-pymo})_2$ (M = Co, $\mathbf{1_H}$, and M = Zn, $\mathbf{2_H}$) were directly precipitated using the parent 2-pymo ligand.[16]

The most remarkable feature of the IR spectra for the $\mathbf{1_X}$ and $\mathbf{2_X}$ species is that the ν(CO) stretching bands appear at lower wavenumbers compared to free 5-X-2-pymo ligands (Table 2). The weakening of the C═O bond can be attributed to intermolecular contacts involving the exocyclic oxygen atom (of the O···X type, as later shown by X-ray diffraction).[27]

The $\mathbf{1_X}$ species are deep purple colored, which is characteristic of tetrahedral $Co^{II}N_4$ chromophores, when the N atoms belong to strongly coordinating heterocyclic anions.[28] Indeed, their electronic spectra show two intense absorption bands (see Experimental Section) corresponding to the $^4A_2 \rightarrow {}^4T_1$ (ν_2) and $^4A_2 \rightarrow {}^4T_1$(P) ($\nu_3$) electronic transitions. At variance, the $^4A_2 \rightarrow {}^4T_2$ (ν_1) one, occurring in the NIR region,

(23) Coelho, A. A. *J. Appl. Crystallogr.* **2000**, *33*, 899−908.
(24) The geometries of the 5-X-2-pymo anions have been optimized at the B3LYP/6-311G(2d, 1p) level of theory (for the iodine atom the basis set 3-21G**+ was adopted) using the following: *Gaussian 03W*, revision C.02: Gaussian, Inc.: Pittsburgh, PA, 2004.
(25) Cheary, R. W.; Coelho, A. A. *J. Appl. Crystallogr.* **1992**, *25*, 109−121.
(26) (a) March, A. *Z. Kristallogr.* **1932**, *81*, 285−297. (b) Dollase, W. A. *J. Appl. Crystallogr.* **1986**, *19*, 267−272.
(27) Preliminary results on the crystal structures of the 5-X-2-pymo ligands (X = Br and I), obtained by XRPD methods, showed X···O contacts slightly above 2.9 Å. The same occurs for the long known chloro derivative (Furberg, S.; Solbakk, J. *Acta Chem. Scand. A* **1974**, *28*, 435). For all these species, the solid-state IR frequencies of the CO stretching fall above 1648 cm^{-1}.
(28) (a) Tian, Y.-Q.; Cai, C.-X. Y.; Ji, Y.; You, X.-Z.; Peng, S.-M.; Lee G.-H. *Angew. Chem., Int. Ed.* **2002**, *41*, 1384−1386. (b) Tian, Y.-Q.; Cai, C.-X.; Ren, X.-M.; Duan, C.-Y.; Xu, Y.; Gao, S.; You, X.-Z. *Chem.*—Eur. J. **2003**, *9*, 5673−5685. (c) Yang, G. *J. Chem. Crystallogr.* **2004**, *34*, 269−274.

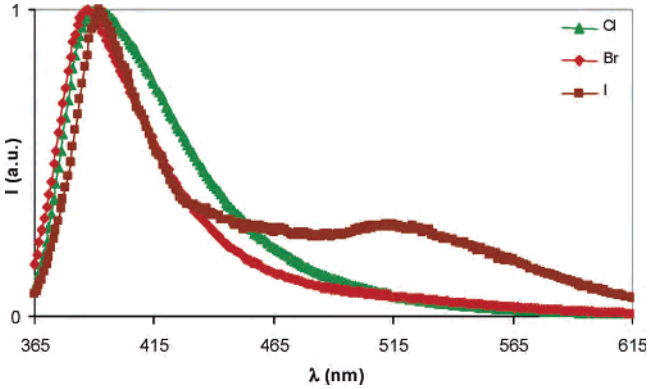

Figure 1. Room-temperature solid-state emission spectra of $[Zn(5\text{-Cl-2-pymo})_2]_n$ (green triangle), $[Zn(5\text{-Br-2-pymo})_2]_n$ (red diamond), and $[Zn(5\text{-I-2-pymo})_2]_n$ (magenta square). The solid lines are only for guiding the eye.

is not detectable. In the case of d^7 tetrahedral complexes, the position of the maximum of the first electronic transition, ν_1, coincides with the value of Δ_t. Yet, being ν_1 undetectable in the spectra of $\mathbf{1_X}$, their values have been calculated from those of ν_2 and ν_3, by applying Dou's method (Table 2).[29] The electron-withdrawing nature of the pyrimidine-2-olate halide substituents is responsible for a slight increase in the Δ_t values compared to that for $\mathbf{1_H}$. The respective values of Racah parameters B for $\mathbf{1_H}$, $\mathbf{1_{Cl}}$, $\mathbf{1_{Br}}$, and $\mathbf{1_I}$ are 755, 762, 717, and 714 cm^{-1}. It should be noted the decrease in the B values according to $\mathbf{1_{Cl}} > \mathbf{1_{Br}} > \mathbf{1_I}$ indicates an increase in the covalent character of the coordinative bond along the series.

We also measured the room-temperature solid-state photoluminescence spectra of the $\mathbf{2_{Cl}}$, $\mathbf{2_{Br}}$, and $\mathbf{2_I}$ species, which resulted in intense emission maxima centered at about 390 nm. An additional, broad band is observed for $\mathbf{2_I}$, centered at about 515 nm (Figure 1). To the best of our knowledge, only two types of electronic transitions have been invoked up to now to describe the lowest (HOMO → LUMO) photoluminescence emission in Zn(II) coordination complexes,[30] namely ligand-to-ligand or ligand-to-metal charge transfers. However, as underlined by Zheng and Chen,[30] and given the number of factors that can play a part in this phenomenon, it is difficult to propose a definitive mechanistic interpretation on the basis of only the emission spectra.

The thermal stability of the title compounds has been investigated by means of DSC and TG measurements. In the case of both the $\mathbf{1_X}$ and $\mathbf{2_X}$ series no distinct events can be detected but decomposition. For the species $\mathbf{1_{Cl}}$, $\mathbf{1_{Br}}$, and $\mathbf{1_I}$, decomposition is responsible for sharp weight losses on the TG diagrams, starting at 420, 450, and 350 °C, respectively. Similar sharp weight losses characterize the TG diagrams of the species $\mathbf{2_{Cl}}$, $\mathbf{2_{Br}}$, and $\mathbf{2_I}$, with T_{dec} of 410, 430, and 330 °C. At least in the case of $\mathbf{1_{Cl}}$, $\mathbf{2_{Cl}}$, $\mathbf{1_{Br}}$, and $\mathbf{2_{Br}}$, these observations once again strengthen our early findings on the high thermal robustness of metal pyrimidin-2-olates, a feature to be taken into consideration when

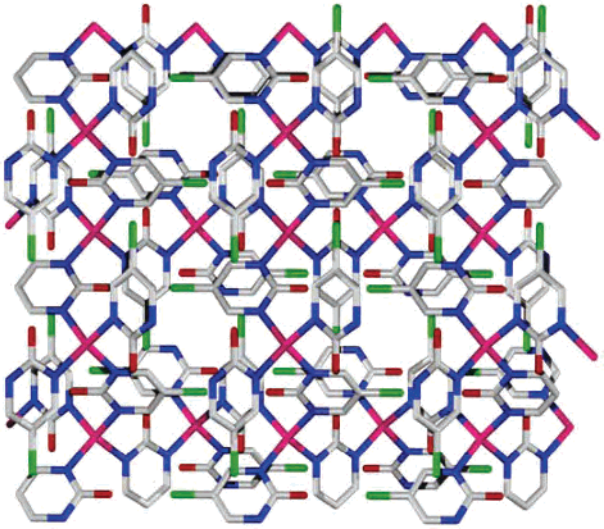

Figure 2. Representation of the packing motif in $[Co(5\text{-Cl-2-pymo})_2]_n$, $\mathbf{1_{Cl}}$, viewed approximately down [001]. At the drawing level, the representations for $\mathbf{1_{Br}}$, $\mathbf{1_I}$, $\mathbf{2_{Cl}}$, $\mathbf{2_{Br}}$, and $\mathbf{2_I}$ are practically indistinguishable. Key: C (gray); N (blue); O (red); halide (green); Co (magenta).

practical applications are searched for. Indeed, decomposition temperatures as high as 560 and 570 °C are reached in the case of $\mathbf{1_H}$ and $\mathbf{2_H}$.[16] The decrease in T_{dec} on passing from **1** to $\mathbf{2_H}$ to **1** to $\mathbf{2_X}$ may be due to the presence of the halides, which facilitate the pyrimidine ring activation during the decomposition process: the dissociation energies of the pyridine−X bond (taken as a model of the present pyrimidine−X one) have indeed values of 464, 405, 337, and 272 kJ mol^{-1} for X = H, Cl, Br, and I, respectively.[31] Despite of the different dissociation energies of the C−Cl and C−Br bonds, our observation leads to an unexpected comparable stability of the chlorine and bromine derivatives (vide infra for a possible structural interpretation).

Crystal Structures and Thermodiffractometric Studies of $[Co(5\text{-X-2-pymo})_2]_n$ ($\mathbf{1_X}$) and $[Zn(5\text{-X-2-pymo})_2]_n$ ($\mathbf{2_X}$) Materials. (a) Crystal Structures. The asymmetric units of the isomorphous $[M(5\text{-X-2-pymo})_2]_n$ compounds are composed by (a portion of) one metal center, lying about a $\bar{4}$ symmetry site (*a* Wyckoff position) and half an organic ligand, lying about a 2-fold axis parallel to *a* or *b* (*d* Wyckoff position) and passing through the exocyclic oxygen and halide atoms. Each metal center, showing a tetrahedral stereochemistry, is coordinated by four nitrogen atoms of four distinct ligands (Figure 2; consult Table 2 for significant bond distances and angles). Not surprisingly, the ligands act in the N,N′-exo-bidentate fashion, bridging metal centers 5.7−5.9 Å apart. Note that, as expected, the trend $M\cdots M(\mathbf{1_X}) < M\cdots M(\mathbf{2_X})$ holds for each halide and can be attributed to the slightly longer tetrahedral ionic radius of Zn(II) vs Co(II) (0.60 vs 0.58 Å).[32]

The N,N′-exo-bidentate coordination mode is, by far, the most common one adopted by the parent 2-pymo ligand[15,16,33] yet not by its 5-nitro derivative. The latter, in the few cases

(29) Dou, Y. *J. Chem. Educ.* **1990**, *67*, 134−134.
(30) Zheng, S. L.; Chen, X.-M. *Aust. J. Chem.* **2004**, *57*, 703−712 and references therein.
(31) McMurry, J. E. *Organic Chemistry*, 6th edition; Brooks Cole: Pacific Grove, CA, 2004; Chapter 5.
(32) Shannon, R. D. *Acta Crystallogr.* **1976**, *A32*, 751−767.
(33) Quirós, M. *Acta Crystallogr.* **1994**, *C50*, 1236−1239.

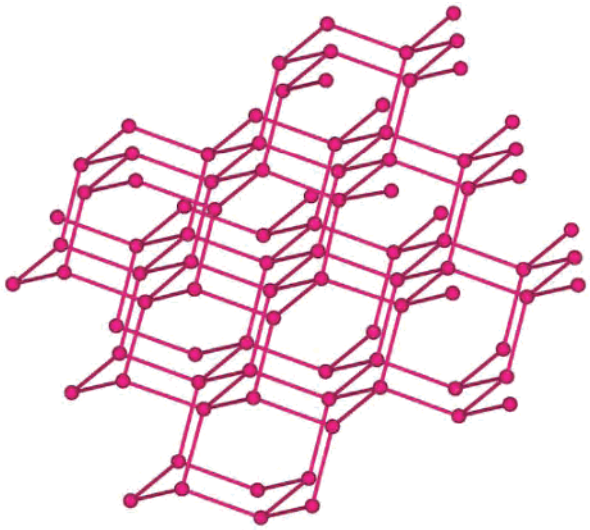

Figure 3. Representation of the three-dimensional diamondoid motif in $[M(5\text{-X-2-pymo})_2]_n$. Metal centers are represented as spheres, and 5-X-2-pymo ligands, as sticks.

in which has been employed, has not infrequently shown its exocyclic oxygen atom coordinated to the metal center.[34]

The bridging mode adopted by the organic moieties results, in both $\mathbf{1_X}$ and $\mathbf{2_X}$, in a non-interpenetrated diamondoid network (see Figure 3, where just the metal centers, taken as vertexes, and the N,N′-bridges, as edges, appear). The same three-dimensional architecture has already been found in the parent $[M(2\text{-pymo})_2]_n$ species (M = Co, Zn).[16] Notably, in the case of $[Ni(2\text{-pymo})_2]_n$, which is *not* isomorphous with the analogues of Co(II) and Zn(II), a diamondoid network can be nevertheless recognized when just the overall connectivity is taken into consideration.[16] At variance, the homoleptic $[M(NP)_2]_n$ derivatives (M = Co, Zn; NP = 5-nitro-2-pyrimidinolate; see Chart 1) deviate from this trend: indeed, they crystallize as two-dimensional slabs in which the metal center shows a MN_3O stereochemistry.[34a]

Within the $\mathbf{1_X}$ and $\mathbf{2_X}$ series the X substituent plays a nonnegligible role on the unit cell volume and on the anisotropic distortion of the crystal lattice. As expected, within a single $\mathbf{1_X}$ or $\mathbf{2_X}$ series, the unit cells inflate on increasing the size of the halide (see Table 2). Yet, due to the special position about which the organic ligands lie (i.e. the C−X vectors being strictly parallel to the crystallographic axes *a* or *b*), the influence of X on the length of the crystallographic axes *a* and *c* is distinct, with *c* surprisingly *shrinking* with increasing the size of the halide (see Figure 4).

This effect can be easily understood with reference to the actual location and symmetry of the bridging 5-X-2-pymo ligands, as described hereafter:

(a) The larger covalent and van der Waals radii of I vs Br and Cl and the orientation of the C−X vectors parallel to *a* (and *b*) induce larger *a* (and *b*) unit cell dimensions for the largest halide (Figure 4 and Table 2).

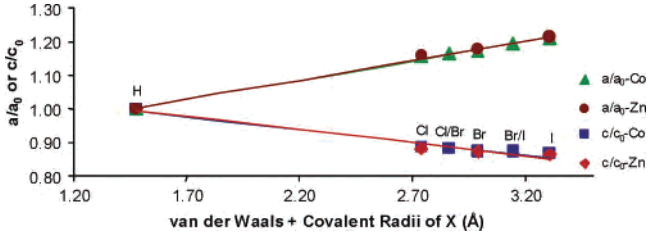

Figure 4. Evolution of *a* (top) and *c* lattice parameters (normalized to those of the $\mathbf{1_H}$ and $\mathbf{2_H}$ species) on varying X in the $[M(5\text{-X-2-pymo})_2]_n$ species (X = H, Cl, Cl/Br, Br, Br/I, and I; M = Co, Zn). The data have been plotted vs the sum of the van der Waals and covalent radii of X (Å). The green triangle, blue square and magenta circle, red diamond refer to Co and Zn, respectively.

(b) 5-X-2-pymo-bridged pairs of metals lie in (x_M, y_M, z_M) and (1/2 + x_M, y_M, 1/4 + z_M), with a d_{MM} intermetallic distance of

$$d_{MM} = [(a\Delta x)^2 + (b\Delta y)^2 + (c\Delta z)^2]^{1/2} = [(a/2)^2 + (c/4)^2]^{1/2}$$

(c) Assuming a substantial constancy of the M−N distances and of the N−M−N angles (witnessed by the values reported in Table 2), d_{MM} should be insensible to the halide nature.

(d) Therefore, the lengthening of *a* must be compensated by the shortening of the *c* axis. This is indeed the effect shown in Figure 4 and in Table 2, where the increase of the cell volume is differently attributed to the coherent changes in *a* and *b* (increasing with halide size) and in *c* (shrinking with it). Notably, even the parent $[M(2\text{-pymo})_2]_n$ analogues (M = Co, Zn) adhere to this scheme.

This system thus appears to be rather flexible, in that it can adapt itself to the large perturbation induced by the 5-X substituents as if it were a pantograph. As a further proof of this behavior, we also successfully precipitated Co(II) species containing an equimolar ratio of either the 5-Cl- and 5-Br-2-pymo ligands or the 5-Br- and 5-I-2-pymo ones. As expected, a (poly)crystalline solid solution was observed in both cases ($\mathbf{1_{Cl/Br}}$ and $\mathbf{1_{Br/I}}$, respectively), with the lattice parameters nicely fitting the observed trends (see Figure 4), with no ligand segregation. These molecular alloys may open the route to the preparation of finely tuned mixed systems, where the properties of the end members can be suitably varied by using the appropriate components in the proper stoichiometry.

The structural features discussed above can be interpreted by observing that, in all species $\mathbf{1_X}$ and $\mathbf{2_X}$, significantly short O···X halogen "bonds",[35] well below 3.0 Å (Table 2), are present along *a* and *b*. In a compilation of halogen bonds characteristics, Metrangolo and Resnati have clearly shown that their strength is higher for the heaviest halides (Cl < Br < I).[36] Thus, the apparent erratic O···X values (Br < Cl < I, Figure 5a) may result from a combination of different and competing factors such as (1) the increase of the atomic size, (2) the increase of the halogen bond strength, and (3) the geometrical restraints imposed by the 3D-framework *but*

(34) (a) Barea, E.; Romero, M. A.; Navarro, J. A. R.; Salas, J. M.; Masciocchi, N.; Galli, S.; Sironi, A. *Inorg. Chem.* **2005**, *44*, 1472−1481. (b) Galli, S.; Masciocchi, N.; Cariati, E.; Sironi, A.; Barea, E.; Haj, M. A.; Navarro, J. A. R.; Salas, J. M. *Chem. Mater.* **2005**, *17*, 4815−4824.

(35) Metrangolo, P.; Neukirch, H.; Pilati, T.; Resnati, G. *Acc. Chem. Res.* **2005**, *38*, 386−395 and references therein.

(36) Metrangolo, P.; Resnati, G. *Chem.*—Eur. J. **2001**, *7*, 2511−2519.

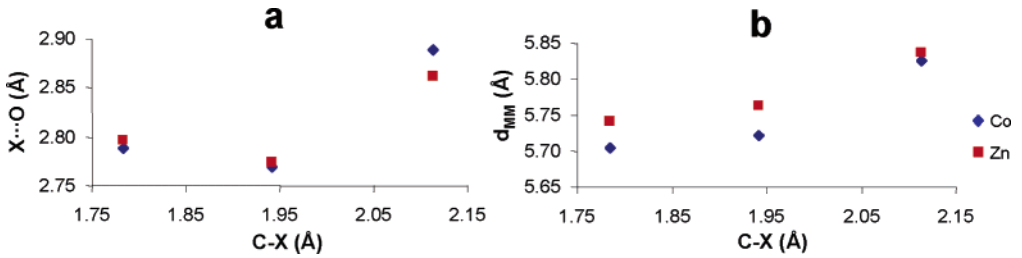

Figure 5. Evolution of (a) X···O (Å) and (b) d_{MM} (Å) as a function of the C−X distance (Å) in the $[M(5\text{-X-2-pymo})_2]_n$ species (X = H, Cl, Br, and I; M = Co, Zn). The blue diamond and red square refer to Co and Zn, respectively.

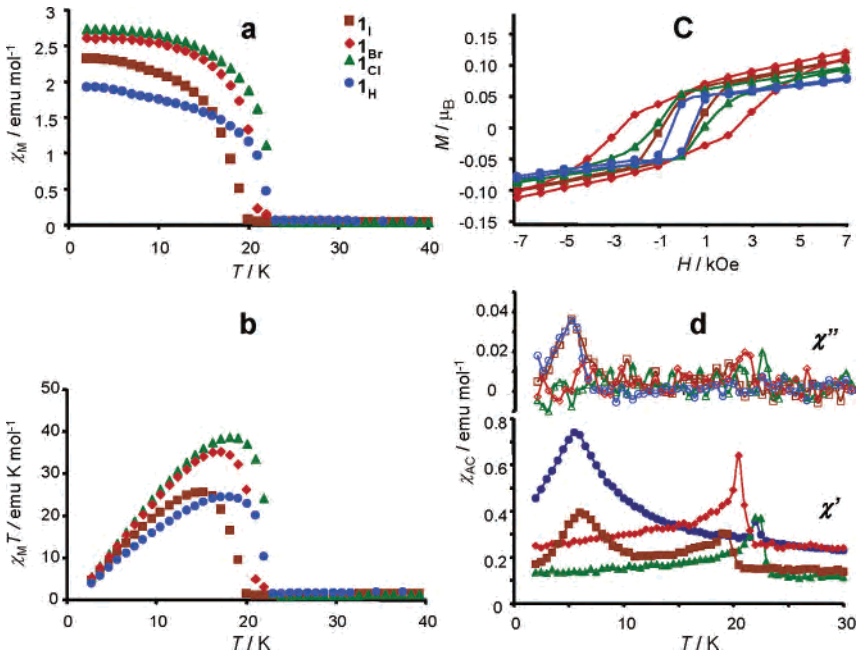

Figure 6. Plots of the thermal behavior of χ_M (a) and $\chi_M T$ (b) with an external magnetic field of 100 Oe for the $\mathbf{1_X}$ materials. (c) Hysteresis loops of $\mathbf{1_X}$ at 2 K. (d) Temperature dependence of the in-phase (χ', full symbols) and the out-of-phase (χ'', open symbols) ac magnetic susceptibilities for $\mathbf{1_X}$.

not from (4) experimental uncertainties.[37] The rather indisputable short O···Br distance in $\mathbf{1_{Br}}$ and $\mathbf{2_{Br}}$, coupled to the independent observations of short M···M contacts (Figure 5b), seems to indicate, in both cases, an optimized situation. This is indeed counterparted by the decomposition temperatures of the $\mathbf{1_{Br}}$ and $\mathbf{2_{Br}}$ species, mentioned above, which are the highest within this class of compounds.

(b) Thermodiffractometric Experiments. In search for information about the dynamics of the ligands within the lattice, we also determined the thermal expansion coefficients on one of the $[M(5\text{-X-2-pymo})_2]_n$ species (namely $\mathbf{2_{Cl}}$; see the Experimental Section for details on the measurements). As supported by the DSC and TG traces, no formation of intermediate phases is observed before decomposition. As emerging from the Le Bail refinements of the acquired diffractograms, on passing from room temperature to 340 °C, the unit cell inflates, because of anisotropic thermal expansion, by about 1.5%, almost exclusively due to an increase of the *c* axis (1.0%, vs 0.3% of *a*). The measured thermal expansion coefficients ($\partial\ln(V)/\partial T = 48 \times 10^{-6}$, $\partial\ln(a)/\partial T = 8 \times 10^{-6}$, and $\partial\ln(c)/\partial T = 30 \times 10^{-6}$ K^{-1}) clearly suggest that, on an increase of the temperature, the 5-X-2-pymo ligands swing preferentially about the M···M hinge, vibrating up and down the *z* direction.

Magnetic Properties of the Cobalt(II) Pyrimidinolate Polymers. The magnetic susceptibility of the microcrystalline samples $\mathbf{1_H}-\mathbf{1_I}$ has been measured at different fields (100, 300, and 5000 Oe) in the temperature range 2−250 K (Figure 6). The thermal dependence of the magnetic susceptibility (χ_M) in the high-temperature region is very similar in all cases, showing a steady increase upon cooling and no dependence with the applied external field. This behavior is consistent with an antiferromagnetic behavior for cobalt(II) systems with a $^4A_2$ ground state. However, in the low-temperature region and below the Néel temperature (T_N = 20−23 K) a clear dependence of the susceptibility with the applied external field is observed, showing a sharp increase in the χ_M values for the 100 Oe (Figure 6a) and 300 Oe measurements. Likewise, the $\chi_M T$ values steadily decrease upon cooling until the Néel temperature T_N = 20−23 K is reached. At lower temperatures, the $\chi_M T$ values sharply increase, with the curves reaching maxima around 15−19 K (Figure 6b).

(37) Because the X···O distance depends essentially on the *well-defined a* lattice parameter; indeed, the crystal packing can be alternatively described by a family of collinear chains of halopymo ligands running along *a* (and *b*), orthogonally interconnected by the metal nodes.

The high temperature ($T > 50$ K) behavior of the magnetic susceptibility for $\mathbf{1_H}-\mathbf{1_I}$ can be fitted to the Curie−Weiss expression

$$\chi_M = C/(T - \Theta) \quad [C = Ng^2\mu^2S(S+1)/3k]$$

obtaining $C = 2.48(1)$ emu K mol^{-1} and $\Theta = -45.3(4)$ K for $\mathbf{1_H}$, $C = 2.53(1)$ emu K mol^{-1} and $\Theta = -42.0(5)$ K for $\mathbf{1_{Cl}}$, $C = 2.51(1)$ emu K mol^{-1} and $\Theta = -45.0(5)$ K for $\mathbf{1_{Br}}$, and $C = 2.58(1)$ emu K mol^{-1} and $\Theta = -43.2(6)$ K for $\mathbf{1_I}$, which agrees with antiferromagnetic exchange taking place through the *N*,*N*′-pyrimidinolate bridges. It should be noted that the nature of the halide substituent does not have any significant effect on the magnetic exchange in the high-temperature range. The μ_{eff} values, calculated from the *C* values obtained from the Curie−Weiss fitting of the magnetic susceptibility (Table 2), are similar (within 2%) to those calculated by taking into account their A_2 state, according to the expression

$$\mu_{eff} = (1 - 4\lambda/\Delta)[4S(S+1)]^{1/2} = (1 - 4\lambda/\Delta)\mu_{eff}^{SO}$$

i.e. 4.357, 4.354, 4.350, and 4.353 μ_B for $\mathbf{1_H}$, $\mathbf{1_{Cl}}$, $\mathbf{1_{Br}}$, and $\mathbf{1_I}$, respectively.[38]

At variance, as previously mentioned, the low-temperature measurements carried out on the $\mathbf{1_H}-\mathbf{1_I}$ materials at different field strengths clearly show that below the Néel temperature, T_N, their magnetic behaviors are highly dependent on the applied field.

The experimental observation of residual magnetic moments at temperatures approaching 0 K can be interpreted by a weak ferromagnetic effect due to spin-canting,[5,39,40] which is allowed despite the high-symmetry crystallographic class and the special location of the magnetic centers: indeed, a thorough symmetry analysis shows that any tilting angle between the spins in the tetragonal plane is possible.[41] For a molecular system isostructural (but not isomorphous) to the $\mathbf{1_H}-\mathbf{1_I}$ ones the same canting effect has been observed.[40b] Magnetic hysteresis studies carried out at 2 K are also consistent with a weak ferromagnetic ordering taking place below the Néel temperature T_N (Figure 6c). However, it should be noted that, despite the related nature of the $\mathbf{1_H}-\mathbf{1_I}$ materials, the area of each hysteresis cycle is markedly different, depending on the functionalization of the pyrimidinolate derivative. Thus, the coercive fields H_{coer} decrease in the following sequence 2500, 1000, 775, and 500 Oe for $\mathbf{1_{Br}}$, $\mathbf{1_{Cl}}$, $\mathbf{1_I}$, and $\mathbf{1_H}$, respectively, whereas the remnant magnetization M_{rem} follows the trend 0.0501 μ_B for $\mathbf{1_{Br}}$ and $\mathbf{1_{Cl}}$, 0.0457 μ_B for $\mathbf{1_I}$, and 0.0358 μ_B for $\mathbf{1_H}$. The spin-canted nature of the magnetic behavior of $\mathbf{1_H}-\mathbf{1_I}$, rather than a regular ferromagnetic behavior, is supported by the fact that the highest magnetizations obtained at 2 K and at an applied field of 50 kOe are significantly lower than the theoretical saturation value of 3 μ_B,[42] namely 0.356, 0.353, 0.412, and 0.408 μ_B for $\mathbf{1_H}$, $\mathbf{1_{Cl}}$, $\mathbf{1_{Br}}$, and $\mathbf{1_I}$, respectively. Taking into account the remnant magnetization values, from the expression $\sin\theta = (M_{rem}/M_{sat}) \times 3$, canting angles in the range 2−3° can be estimated for compounds $\mathbf{1_H}-\mathbf{1_I}$.[40] The sharp rise in the susceptibility values below 20−23 K is accompanied by both real and imaginary components of the ac-susceptibility measured in a 1 Oe field oscillating at 1200 Hz centered at 22, 22.5, 20.5, and 19 K for $\mathbf{1_H}$, $\mathbf{1_{Cl}}$, $\mathbf{1_{Br}}$, and $\mathbf{1_I}$, respectively (Figure 6d), which are due to the spin-canting phenomena. In addition, the $\mathbf{1_H}$ and $\mathbf{1_I}$ ac curves have anomalous real and imaginary components at about 6 K, which may be attributed to an additional long range ordering taking place.[43]

The peculiar magnetic behavior of the $\mathbf{1_H}-\mathbf{1_I}$ materials can be related to the synergistic effects exerted by the acentric crystal structure, the magnetic anisotropy of the cobalt(II) centers, and the anisotropic structural distortions introduced by the 5-substituents of the pyrimidine-2-olate bridges. The lack of a monotonic behavior of the magnetic properties (vs the atomic number or the electronegativity of the X-substituent) described above cannot be rationalized; however, as commented below, it must be related to the overall anomalous performances of the bromine derivatives.

Nonlinear Optical Properties. Testing the second harmonic generation (SHG) efficiencies on unsieved powders of the $\mathbf{1_X}$ and $\mathbf{2_X}$ series (X = Cl, Br, and I) via the Kurtz−Perry powder method,[44] working with an incident wavelength of 1907 nm, resulted in almost undetectable signals with respect to standard urea. As a consequence, a quantitative evaluation of the efficiency of the single species is not available. Thus, the only achievable information is a rough division into two categories when the signal of urea is saturated, the $\mathbf{2_X}$ compounds always showing a higher response than the $\mathbf{1_X}$ ones.[45,46] The weakness of the SHG signals for such highly polarizable ligands can be interpreted on a structural basis since, for symmetry reasons, the X−Ar−O "dipole" cannot concur to the bulk hyperpolarizability tensor.

Indeed, using the approximation proposed by Zyss et al.,[47] according to the $\bar{4}2m$ crystallographic class of the $\mathbf{1_X}$ and $\mathbf{2_X}$

(38) Jolly W. L. *The Synthesis and Characterisation of Inorganic Compounds*; Prentice Hall: Englewood, N.J., 1970.
(39) (a) Rettig, S. J.; Sánchez, V.; Storr, A.; Thompson, R. C.; Trotter, J. *J. Chem. Soc., Dalton Trans.* **2000**, 3931−3937. (b) Rettig, S. J.; Thompson, R. C.; Trotter, J.; Xia, S. *Inorg. Chem.* **1999**, *38*, 1360−1363. (c) Hernández-Molina, M.; Lloret, F.; Ruiz-Pérez, C.; Julve, M. *Inorg. Chem.* **1998**, *37*, 4131−4135. (d) Zeng, M.-H.; Zhang, W.-X.; Sung, X.-Z.; Chen, X.-M. *Angew. Chem., Int. Ed.* **2005**, *44*, 3079−3082. (e) Galán-Mascarós, J. R.; Dunbar, K. R. *Angew. Chem., Int. Ed.* **2003**, *42*, 2289−2293.
(40) See e.g.: (a) Nakayama, K.; Ishida, T.; Takayama, R.; Hashizume, D.; Yasui, M.; Iwasaki, F.; Nogami, T. *Chem. Lett.* **1998**, 497−498. (b) Feyerherm, R.; Loose, A.; Ishida, T.; Nogami, T.; Kreitlow, J.; Baabe, D.; Litterst, F. J.; Sullow, S.; Klauss, H. H.; Doll, K. *Phys. Rev. B* **2004**, *69*, 134427.
(41) Boehm, M.; Roessli, B.; Schefer, J.; Ouladdiaf, B.; Amato, A.; Baines, C.; Staub, U.; Petrakovskii, G. A. *Physica B* **2002**, *318*, 277−281.
(42) Carlin, R. L. *Magnetochemistry*; Springer-Verlag: Berlin, 1986.
(43) Salahn, M. B.; Vilminot, S.; André, G.; Bourée-Vigneron, F.; Richard-Plouet, M.; Mhiri, T.; Kurmoo, M. *Chem. Mater.* **2005**, *17*, 2612−2621.
(44) Kurtz, S. K.; Perry, T. T. *J. Appl. Phys.* **1968**, *39*, 3798−3813.
(45) In the case of $\mathbf{1_H}$ and $\mathbf{2_H}$, slightly better performances and the opposite trend were observed (16), yet using a different incident wavelength (1064 nm), at which the efficiency of the purple-colored Co(II) species might be overestimated, due to contributions from fluorescence emissions. New measurements were thus performed at 1907 nm: a "new" $\mathbf{2_H} > \mathbf{1_H}$ trend was now detected, nicely reproducing the general $\mathbf{2_X} > \mathbf{1_X}$ one here determined.
(46) For the sake of completeness, it must be said that the $\mathbf{2_X}$ species (X = Cl, Br, and I) photodecompose.

species, the only nonvanishing component of the bulk second-order nonlinearity/molecule (b_{eff}) has the expression $b_{eff} = \beta_{CT} \sin \psi \cos \psi \sin^2 \theta \cos \theta$, ψ and θ being the polar coordinates of β_{CT}, the molecular hyperpolarizability. If the X−Ar−O "dipole" is taken as the major charge-transfer axis (CT) of the system, θ (90°) and ψ (either 0 or 90°) imply $b_{eff} = 0$. Consequently, our scarce, but nonzero, signal arises from other electronic transitions which are not symmetry-forbidden, possibly involving the metal centers.

Conclusions

In this report we have shown the fine-tuning of the structural and physicochemical properties (thermal stability and magnetic hardness) of a series of isomorphous, diamondoid frameworks of the $[M(5\text{-X-2-pymo})_2]_n$ type by varying the halide substituent in the 5 position of the pyrimidine ring. The steric demand of these substituents is responsible for a slight perturbance of the crystal cell parameters but not for a change in either the coordination of the metal center or the overall framework topology.

In all isomorphous frameworks, the pyrimidinolates transmit the antiferromagnetic coupling between the Co(II) ions; however, the uncompensated antiferromagnetic couplings arising from the diamondoid topology [as in Co(4-azabenzimidazolate)$_2$[39a]] leads to spin-canting phenomena that are sensitive to the structural characteristics. Indeed, a significant enhancement of the magnetic hardness takes place in the halo-substituted derivatives compared to the pristine $\mathbf{1_H}$ species.

Another remarkable feature of these materials is their high thermal stability: although lower than the pristine $[M(2\text{-pymo})_2]_n$, it is still considerably high even in the case of the most activated ones, $\mathbf{1_I}$ and $\mathbf{2_I}$.

Interestingly, halogen bond strength, thermal decomposition temperatures, and magnetic measurements coherently indicate that the bromo derivatives enhance these functional properties, thus showing that halide substitution does not imply monotonic changes of these physicochemical features.

The values of the halogen bond interactions also explain why the $[M(5\text{-nitro-2-pymo})_2]_n$[34a] materials necessarily adopt a different structure: no space would be left in the rather dense diamondoid packing for the bulkier nitro group. It would be therefore interesting to prepare 5-amino- or 5-hydroxy-substituted pyrimidinols (with smaller X subsituents), to verify the possibility of building extended frameworks, isomorphous to $\mathbf{1_X}-\mathbf{2_X}$, containing linear chains of H-bonded motifs.

Acknowledgment. We thank the suggestions of Prof. E. Colacio on the magnetic properties of the $\mathbf{1}_X$ materials. The Spanish and Italian Ministries of Education and Science (Acción Integrada HI2003-0081, CTQ-2005-00329/BQU, Ph.D. doctoral fellowships (M.A.G. and E.B.), E.B. Postdoctoral Grant (EX2005-1004)) and Junta de Andalucia are acknowledged for funding. We are deeply indebted to the reviewers, who provided suggestions that allowed us to improve the quality of the manuscript.

Supporting Information Available: Final Rietveld refinement plots for species $\mathbf{1_X}$ and $\mathbf{2_X}$ (X = Cl, Br, and I). This material is available free of charge via the Internet at http://pubs.acs.org.

IC0602188

(47) (a) Zyss, J.; Oudar, J. L. *Phys. Rev. A* **1982**, *26*, 2028. (b) Zyss, J.; Chemla, D. S. *Nonlinear Optical Properties of Organic Molecules and Crystals*; Chemla, D. S., Zyss, J., Eds.; Academic Press, Inc.: Orlando, FL, 1987; Vol. 1, pp 23−187.